Electronic Supplementary Information (ESI)

Tellurate Polymorphs with High-performance Nonlinear Optical Switch Property and Wide Mid-IR Transparency

Dan Wang,[†] Yunxi Zhang,[†] Qi Shi,[†] Qian Liu,[†] Daqing Yang,[†] Bingbing Zhang,[†] and Ying Wang[†,*]

[†] College of Chemistry and Environmental Science, Hebei University, 180 East Wusi Road, Baoding 071002, China. Email: wangy@hbu.edu.cn

Table of Contents

Experimental Procedures

Synthesis. All the reagents are analytical grade and gained from Aladdin without further processing and purification. Single crystals of β-Li_2HfTeO_6 were obtained by using the high-temperature flux method. The mixture of Li_2CO_3, HfO_2, and TeO_2 in a molar ratio of 3:1:5 was fully ground and placed in a platinum crucible. The crucible was heated to 750 °C in 3 h, and held at this temperature for 24 h. Afterward, the solution was cooled slowly to 620 °C with a rate of 2 °C·h^{-1}, and then cooled down to room temperature quickly. Colorless crystals of β-Li_2HfTeO_6 were obtained from the crushed products. However, under similar conditions, the attempts to obtain single crystals of α-Li_2HfTeO_6 were failed due to poor crystallinity.

The polycrystalline samples of α-Li_2HfTeO_6 were obtained by the solid-state reaction method in the air in three steps. First, according to equation **1**, Li_2CO_3 and HfO_2 with a stoichiometric ratio were weighted and fully grounded. The mixture was loaded into a corundum crucible and heated to 1000 °C at a rate of 5 °C·min^{-1}, held at this temperature for 14 hours to obtain Li_2HfO_3. Second, Li_2HfO_3 and TeO_2 combine with oxygen from the air to create Li_2HfTeO_6 as suggested by equation **2**. The mixture was heated at 700 °C for 12 h and 650 °C for 12 h, respectively, with several intermittent grindings. At this stage, a weak SHG signal can be detected from the as-obtained products, suggesting that both α-Li_2HfTeO_6 and β-Li_2HfTeO_6 exist. Finally, to prepare single phase of α-Li_2HfTeO_6, the sample was heated again at 550 °C for 2 d and slowly cooled to room temperature in 24 h.

$$Li_2CO_3 + HfO_2 \rightarrow Li_2HfO_3 \quad \textbf{(1)}$$
$$Li_2HfO_3 + TeO_2 + 1/2O_2 \rightarrow Li_2HfTeO_6 \quad \textbf{(2)}$$
$$H_6TeO_6 \rightarrow TeO_3 + 3H_2O \quad \textbf{(3)}$$
$$Li_2HfO_3 + TeO_3 \rightarrow Li_2HfTeO_6 \quad \textbf{(4)}$$

Powder samples of β-Li_2HfTeO_6 were prepared in a similar way with some differences in Te source and temperature control. Step 1: Li_2HfO_3 was pre-synthesized as described above. Step 2: H_6TeO_6 was calcined at 400 °C for 12h to synthesize TeO_3 (equation **3**). Step 3, the as-obtained Li_2HfO_3 and TeO_3 in the equal molar ratio were calcined at 750 °C for 48 h with several intermittent grindings (equation **4**), and the sample was cooled to the room temperature by taking it out of the furnace directly and cooled in ice water to bypass the phase transition. The phase purity was checked by XRD and SHG tests.

Single-Crystal XRD. The crystal data were collected on a Bruker D8 VENTURE diffractometer. The diffractometer was equipped with a microfocus sealed X-ray tube and used Mo K_α radiation (λ = 0.71073 Å). The data reduction and multi-scan absorption correction were performed using the SAINT and SADABS, respectively. Within Olex2 software,[1] the structure was solved and refined by ShelXT[2] and ShelXL,[3] respectively. The crystal symmetry was checked by PLATON.[4] The information of crystal data and detailed refinement are summarized in Table S1. The atomic coordinates, isotropic displacement parameters, and bond valence sums of each atom are presented in Table S2. The selected bond lengths are given in Table S3.

Powder XRD. Powder XRD measurements were performed on a D8 advance X-ray diffractometer with Cu K_α radiation (λ = 1.5408 Å) at room temperature. The diffraction patterns were scanned with the 2θ range from 10˚ to 70˚. The scan step width was 0.02˚ and the scan time was 2-5 s. Rietveld refinement of the structural model was performed by GSAS-II software.[5]

Thermal Analysis. The thermal gravimetric (TG) analysis and differential scanning calorimetry (DSC) of Li_2HfTeO_6 were measured with a NETZSCH5 instrument under the air. The sample was heated from 30 °C to 1100°C with a heating rate of 10K/min at an alumina crucible.

Supporting Information

Scanning Electronic Microscope (SEM) Images and Energy Dispersive X-Ray (EDX) Microanalysis. SEM images and EDX microanalysis of the crystals were performed on a Hitachi TM4000Plus microscopes with acceleration voltage of 15 kV. In addition, the elemental mapping images were recorded to show the distribution of chemical elements.

UV-Vis-NIR Diffuse-Reflectance Spectrum. Polycrystalline samples were used for diffuse-reflectance spectrum measurements. A METASH UV-6100 spectrophotometer was used to measure the diffuse reflectance spectrum in the 200-1100 nm wavelength range at room temperature.

Infrared Spectroscopy. The IR spectrum was measured by Shimadzu IR Affinity-1 Fourier transform infrared spectrometer at room temperature in the range of 400-4000 cm^{-1}. Pellets for measurement were prepared by pressing a thoroughly ground mixture of 5 mg sample and 500 mg dried KBr.

Dielectric Spectrum. Polycrystalline samples of α-Li_2HfTeO_6 were cold-pressed into a pellet (~12 mm diameter and ~1.3 mm thick), and then sintered at 700 °C for 48 h. The silver paste was applied to both sides of the sintered pellet. The temperature-dependent dielectric spectrum was recorded with a TH2827A Precision LCR Meter. The changes of the dielectric coefficient at variable temperatures (50 to 800 °C, at a heating rate of 2 °C·min^{-1}) were recorded in the frequency range from 10 KHz to 1 MHz.

SHG Measurement. The SHG effects of the powder samples were measured by using a modified Kurtz and Perry method with a Q-switched 1064 nm Nd: YAG laser.[6] The samples were ground and divided into fractions according to different particle size ranges: 20-38.5, 38.5-55, 55-80, 80-125, 125-160, 160-200, and 200-250 μm. The same particle-sized KDP samples were used as the standard. Temperature-dependent analysis of SHG effects was performed using ground powder from 50 to 700 °C. The SHG switching contrast is defined as the ratio of the SHG intensities at the ON and OFF status near the phase transition temperature.

Ferroelectric Measurements. The polarization of α-Li_2HfTeO_6 was measured at room temperature by using a ZT-1B ferroelectric test system. The measurements were performed at a fixed frequency of 10 Hz with electric fields ranging from 25 to 100 kV cm^{-1}.

LDT Measurement. The optical damage induced by laser was tested on crystalline powder pellet samples using a Q-switched 1064 nm Nd: YAG laser (1064 nm, 7 ns, 5 Hz). The pulse energy was changed from 20-100 mJ and a convex lens was used to adjust the beam diameter. The damaged area can be directly observed under a microscope.

Theoretical Calculation. Theoretical calculations were performed by using the CASTEP package based on density functional theory (DFT).[7, 8] Perdew-Burke-Ernzerhof generalized gradient approximation (PBE-GGA) functional was adopted to describe the exchange-correlation energy.[9] The energy cut-off for the plane-wave basis was set to be 750 eV. The Norm-conserving pseudopotential (NCP) was adopted with following valence electrons, Li ($2s^1$), Hf ($5d^2 6s^2$), Te ($5s^2 5p^4$), O ($2s^2 2p^4$). The numerical integration of the Brillouin zone was performed using a Monkhorst-Pack scheme with *k*-point grid density of 3 × 3 × 2. In addition, a scissors operator was adopted to correct the underestimation of band gap induced by PBE-GGA. On the basis of the scissor-corrected electron band structure, the second order NLO coefficients d_{ij} were calculated using the length-gauge formalism at a zero-frequency limit.[10] The static second-order nonlinear susceptibilities can be ascribed to virtual-electron and virtual-hole processes. In addition, the SHG-weighted electron density method was adopted to visualize the contribution of each atom to the SHG response.[11, 12]

Results and Discussion

Table S1. Crystal data and structure refinement for α-Li_2HfTeO_6 and β-Li_2HfTeO_6.

Empirical formula	**α-Li_2HfTeO_6**	**β-Li_2HfTeO_6**	
Formula weight	415.97	Formula weight	415.97
Crystal system	Trigonal	Crystal system	Trigonal
Space group (number)	$R3$ (146)	Space group (number)	$R\overline{3}$ (148)
a [Å]	5.1615	a [Å]	5.153(3)
b [Å]	5.1615	b [Å]	5.153(3)
c [Å]	13.7822	c [Å]	13.753(14)
Volume [Å^3]	317.9	Volume [Å^3]	316.3(5)
Z	3	Z	3
ρ_{calc} [gcm^{-3}]	6.516	ρ_{calc} [gcm^{-3}]	6.552
Radiation	CuK_α (λ = 1.5408 Å)	μ [mm^{-1}]	31.454
Instrument type	Bragg-Brentano	F(000)	534
R_{wp}	0.0889	Crystal colour	colourless
R_p	0.0690	Crystal shape	block
Phase fraction	0.980	Radiation	MoK_α (λ = 0.71073 Å)
		2Θ range [°]	8.89 to 55.01 (0.77 Å)
		Index ranges	$-6 \le h \le 6$, $-6 \le k \le 5$, $-17 \le l \le 16$
		Reflections collected	1193
		Independent reflections	165, R_{int} = 0.0478, R_{sigma} = 0.0275
		Completeness	100.0 %
		Data / Restraints / Parameters	165/12/19
		Goodness-of-fit on F^2	1.311
		Final R indexes [$I \ge 2\sigma(I)$]	R_1 = 0.0257, wR_2 = 0.0586
		Final R indexes [all data]	R_1 = 0.0279, wR_2 = 0.0589
		Largest peak/hole [eÅ^{-3}]	1.75/-1.28
		Extinction coefficient	0.0051(8)

Table S2. Atomic coordinates and U_{eq} [Å^2] for α-Li_2HfTeO_6 and β-Li_2HfTeO_6.

Atom	*x*	*y*	*z*	U_{eq}[a]	BVS[b]
			α-Li_2HfTeO_6		
Li(1)	2/3	1/3	0.4395	0.0487	0.84
Li(2)	0	0	0.5934	0.0064	0.92
Hf(1)	0	0	0.3759	0.0044	4.34
Te(1)	1/3	2/3	0.5456	0.0043	6.11
O(1)	0.3527	0.0581	0.2966	0.0368	2.05
O(2)	0.2844	0.33796	0.4697	0.0020	2.01
			β-Li_2HfTeO_6		
Li(1)	1	1	0.232	0.0660	0.84
Hf(1)	2/3	1/3	1/3	0.0060	4.23
Te(1)	1/3	2/3	1/6	0.0062	5.92
O(1)	0.6200	0.6321	0.2469	0.0157	1.97

[a] U_{eq} is defined as 1/3 of the trace of the orthogonalized U_{ij} tensor.

[b] Bond valence sums (BVS) are calculated by using bond-valence theory ($S_i = \exp[(R_o - R_i/B]$, where R_o is an empirical constant, R_i is the length of bond *I* (in angstroms), and B= 0.37).

Table S3. Selected bond lengths [Å] for α-Li_2HfTeO_6 and β-Li_2HfTeO_6.

α-Li_2HfTeO_6		**β-Li_2HfTeO_6.**	
Li(1)–O(1) $\times 3$	2.4939	Li(1)–O(1) $\times 3$	1.939
Li(1)–O(2) $\times 3$	2.0281	Li(1)–O(1) $\times 3$	2.600
Li(2)–O(1) $\times 3$	2.0356	Hf(1)–O(1) $\times 6$	2.053
Li(2)–O(2) $\times 3$	2.3553	Te(1)–O(1) $\times 6$	1.922
Hf(1)–O(1) $\times 3$	2.0127		
Hf(1)–O(2) $\times 3$	2.0756		
Te(1)–O(1) $\times 3$	1.9214		
Te(1)–O(2) $\times 3$	1.9001		

Table S4. Comparison of structure and optical properties of compounds in Li_2MTeO_6 (M = tetravalent cation) family.

	space group	octahedral distortion Δd		SHG (× KDP)	transparent region (μm)	LDT (MW cm^{-2})
		MO_6	TeO_6			
Li_2TiTeO_6	*Pnn*2	0.20	0.06	26	0.38-6.72	>550
Li_2ZrTeO_6	*R*3	0.12	0.02	2.5	0.29-7.4	>1300
α-Li_2HfTeO_6	*R*3	0.19	0.06	2.2	0.27-8.6	>1000
β-Li_2HfTeO_6	$R\bar{3}$	0	0	/	0.26-8.6	>1000
Li_2SnTeO_6	*Pnn*2	0.01	0.09	2.5	0.38-6.86	>672

Table S5. Displacive mode amplitudes [Å] from β-Li_2HfTeO_6 to α-Li_2HfTeO_6.

mode	atom	A_s	A_p	d_{max}	Description
Γ_1^+	Li(1)_ A(a)	0.22633	0.22633	0.16004	Shift of Li and O atoms, **CS**
	O(1)_ A_1(a)	-0.10135	-0.10135	0.04138	
	O(1)_ A_2(a)	-0.05727	-0.05727	0.02338	
	O(1)_ A_3(a)	-0.00292	-0.00292	0.00119	
	all	**0.25453**	**0.25453**	/	
Γ_1^-	Li(1)_ A(a)	0.00000	0.00000	0.00000	/
	Hf(1)_ Au(a)	0.35849	0.35849	0.35849	Displacement of Hf atom, **NCS**
	Te(1) _ Au(a)	0.40131	0.40131	0.40131	Displacement of Te atom, **NCS**
	O(1)_ A_1(a)	0.05569	0.05569	0.02274	Shift of O atoms, **NCS**
	O(1)_ A_2(a)	-0.06093	-0.06093	0.02487	
	O(1)_ A_3(a)	1.12304	1.12304	0.45848	Rotation of HfO_6/TeO_6 octahedron, **NCS**
	all	**1.24804**	**1.24804**	/	
Overall		**1.27373**	**1.27373**	/	

Note: The magnitude of A_s is the square root of the sum of the squares of the mode-induced changes within the primitive supercell (i.e. the root-summed-squared displacement). $A_p = A_s$*sqrt(V_p/V_s) to be normalized to the parent cell, where V_p and V_s are the respective primitive parent and supercell volumes. d_{max} is the maximum displacive mode amplitude. CS = centrosymmetric transform; NCS = noncentrosymmetric transform.

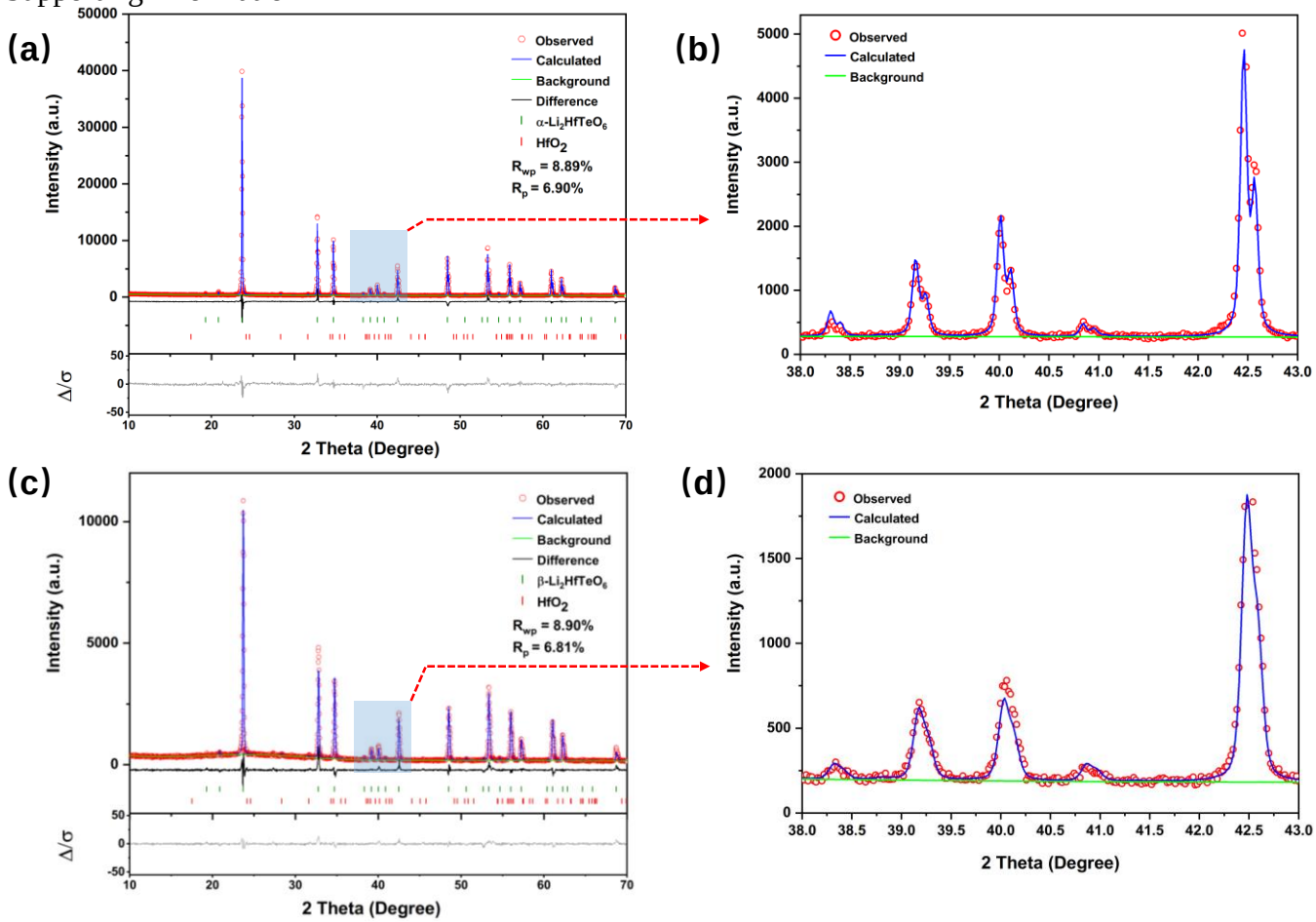

Figure S1. Rietveld refinement of the powder XRD data for (a)-(b) α-Li_2HfTeO_6 and enlarged area from 38 to 43°, and (c)-(d) β-Li_2HfTeO_6 and enlarged area from 38 to 43°. Note that a small quantity of HfO_2 (1.9% and 1.6%, for α-Li_2HfTeO_6 and β-Li_2HfTeO_6, respectively) coexists as the impurity, which cannot be avoided after plenty of attempts. On first sight, the two polymorphs show almost the same XRD pattern. However, when zoom in on curves between 38 to 43°, one can see that several peaks of α-Li_2HfTeO_6 are split while those of β-Li_2HfTeO_6 are not divided. The is in line with the systematic absence law of XRD: β-Li_2HfTeO_6 with higher symmetry shows less diffraction peaks than α-Li_2HfTeO_6 due to the extinction rule.

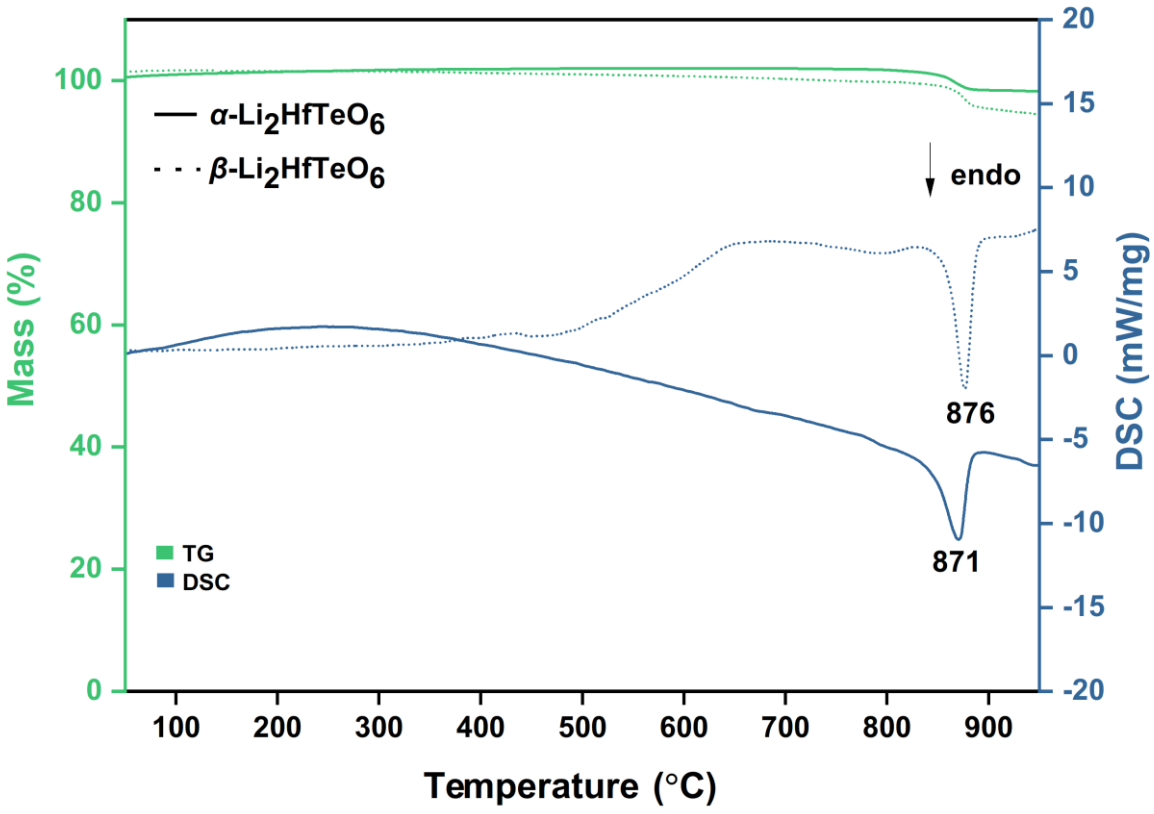

Figure S2. TG and DSC curve of Li_2HfTeO_6 polymorphs.

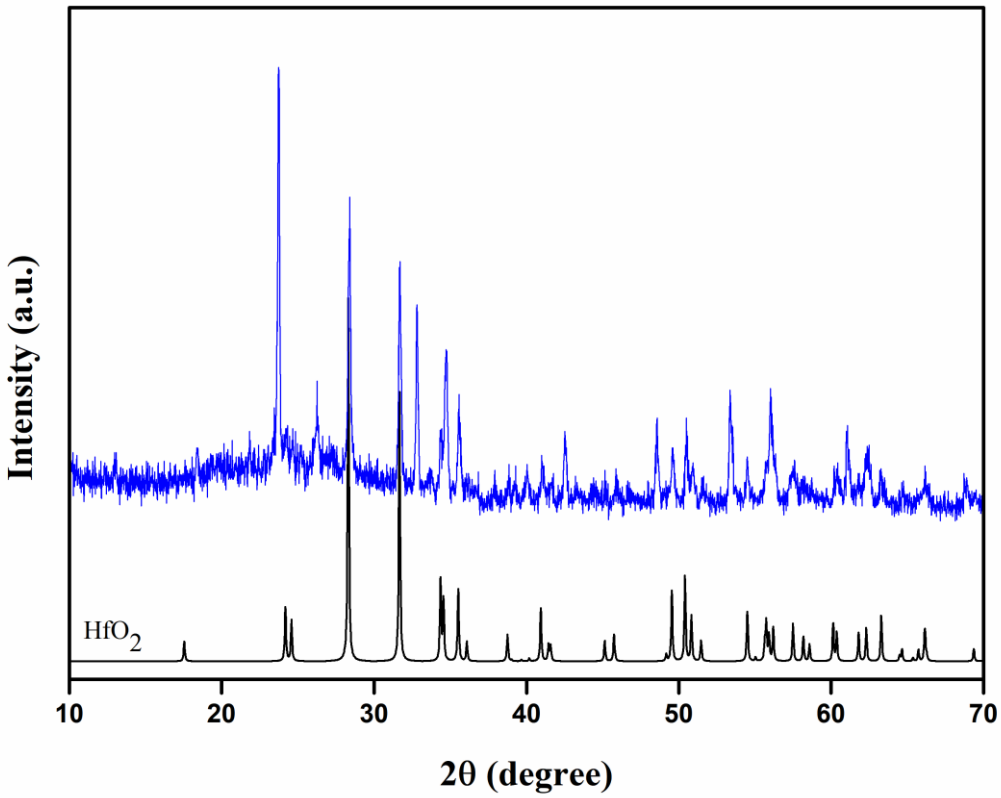

Figure S3. XRD pattern of Li_2HfTeO_6 after heating to 850 °C. The main decomposition product is HfO_2.

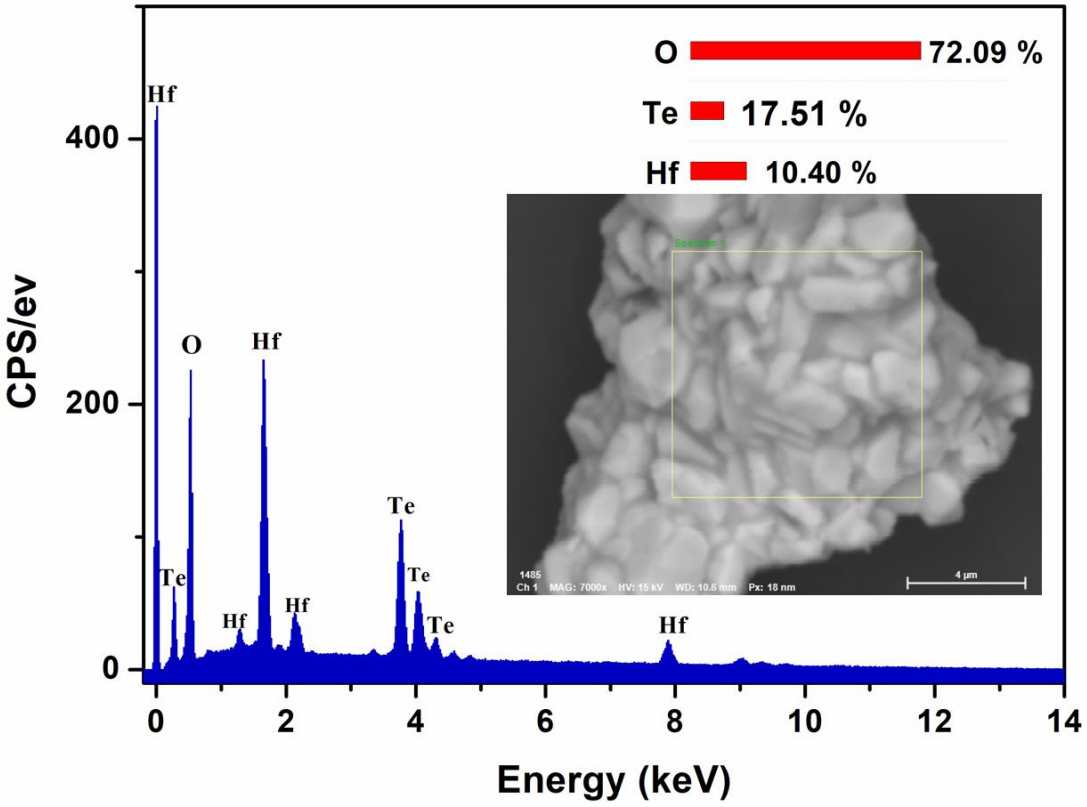

Figure S4. SEM images and EDX microanalysis for β-Li_2HfTeO_6. Noted that the EDX only provides semi-quantitative results, and the Li elements are ignored.

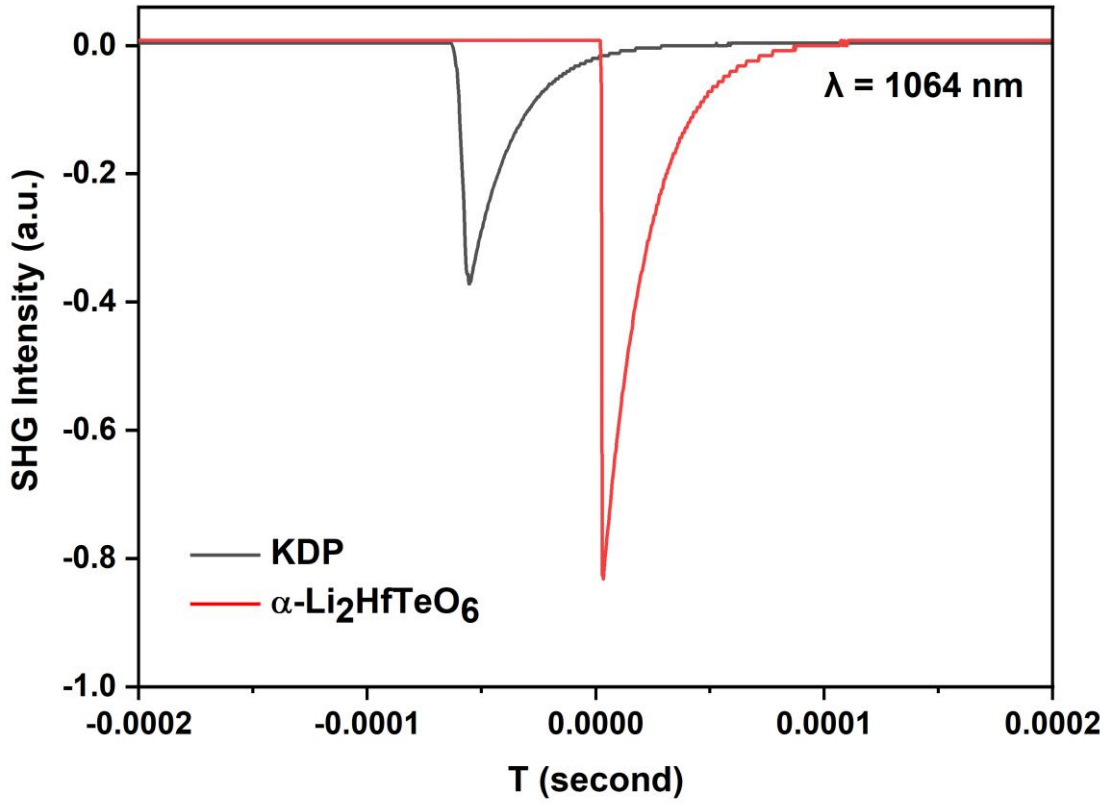

Figure S5. Oscilloscope traces shwoing the SHG intensities for the powder KDP and α-Li_2HfTeO_6.

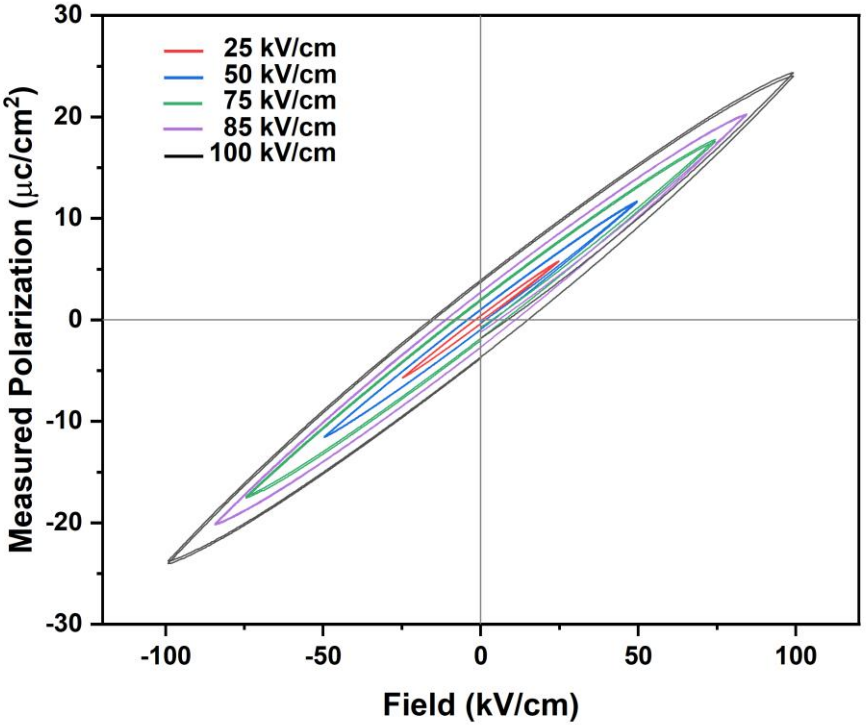

Figure S6. Polarization *vs*. voltage plot for α-Li_2HfTeO_6. Although the curves reveal hysteresis loops, the observed loops do not represent ferroelectric behavior, but dielectric loss.[13, 14]

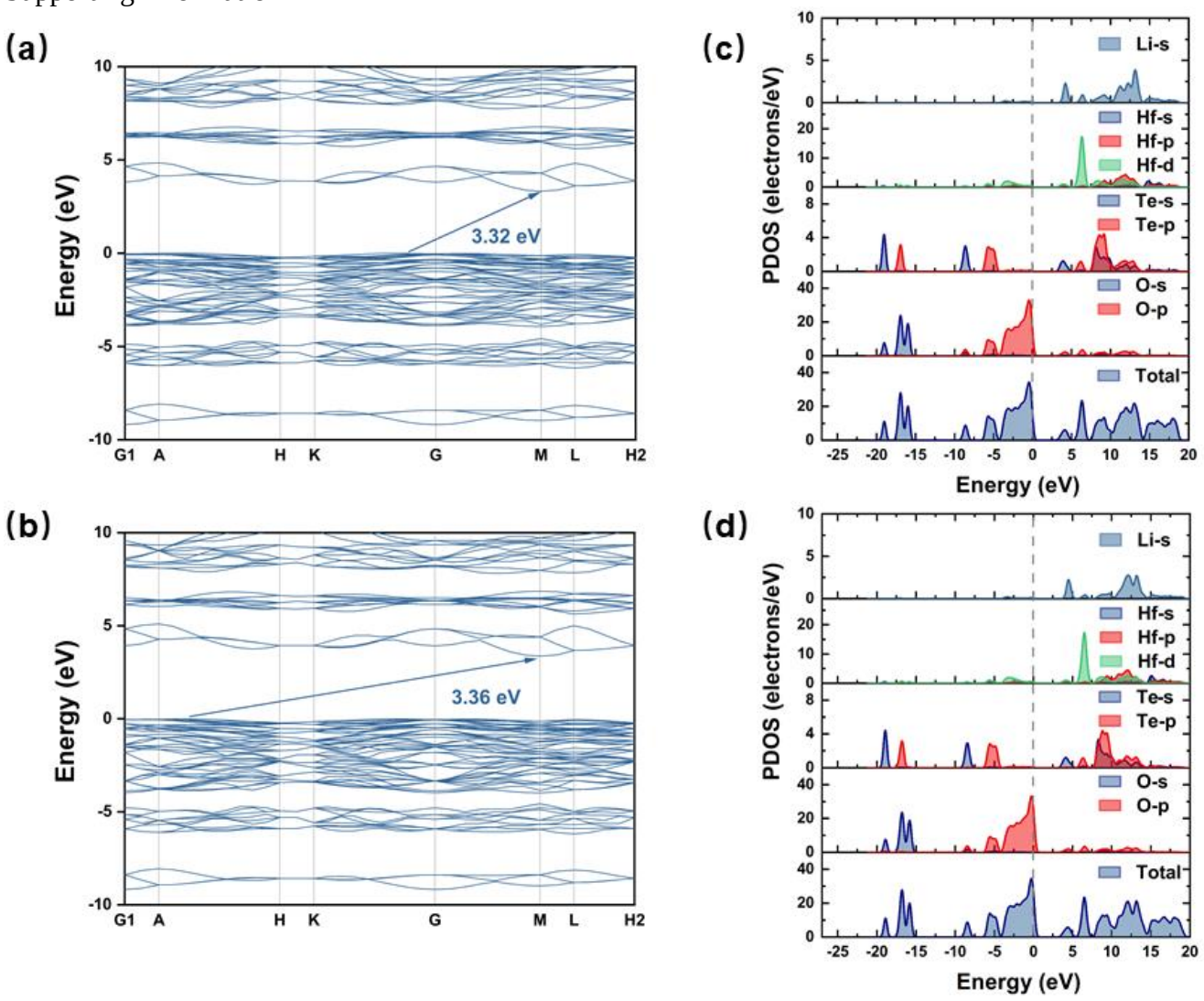

Figure S7. Bandgap of (a) α-Li_2HfTeO_6 and (b) β-Li_2HfTeO_6. The PDOS of (c) α-Li_2HfTeO_6 and (d) β-Li_2HfTeO_6.

.

References

1. O. V. Dolomanov, L. J. Bourhis, R. J. Gildea, J. A. K. Howard and H. Puschmann, OLEX2: A complete structure solution, refinement and analysis program, *J. Appl. Crystallogr.*, 2009, **42**, 339–341.
2. G. Sheldrick, SHELXT - Integrated space-group and crystal-structure determination, *Acta Cryst. A*, 2015, **71**, 3–8.
3. G. Sheldrick, Crystal structure refinement with SHELXL, *Acta Cryst. C*, 2015, **71**, 3–8.
4. A. L. Spek, Single-crystal structure validation with the program PLATON, *J. Appl. Crystallogr.*, 2003, **36**, 7–13.
5. B. H. Toby and R. B. Von Dreele, GSAS-II: The genesis of a modern open-source all purpose crystallography software package, *J. Appl. Crystallogr.*, 2013, **46**, 544–549.
6. S. K. Kurtz and T. T. Perry, A powder technique for the evaluation of nonlinear optical materials, *J. Appl. Phys.*, 1968, **39**, 3798–3813.
7. J. Heyd and G. E. Scuseria, Efficient hybrid density functional calculations in solids: assessment of the Heyd-Scuseria-Ernzerhof screened Coulomb hybrid functional, *J. Chem. Phys.* , 2004, **121**, 1187–1192.
8. V. Milman, K. Refson, S. J. Clark, C. J. Pickard, J. R. Yates, S. P. Gao, P. J. Hasnip, M. I. J. Probert, A. Perlov and M. D. Segall, Electron and vibrational spectroscopies using DFT, plane waves and pseudopotentials: CASTEP implementation, *J. Mol. Struct*, 2010, **954**, 22–35.
9. John P. Perdew, Kieron Burke and M. Ernzerhof, Generalized gradient approximation made simple, *Phys. Rev. Lett.*, 1996, **77**, 3865–3868.
10. S. N. Rashkeev., W. R. L. Lambrecht. and B. Segall., Efficient *ab* initio method for the calculation of frequency-dependent second-order optical response in semiconductors, *Phys. Rev. B*, 1998, **57**, 3905–3919.
11. H. K. Liu, Y. Wang, B. B. Zhang, Z. H. Yang and S. L. Pan, $CsAlB_3O_6F$: A beryllium-free deep-ultraviolet nonlinear optical material with enhanced thermal stability, *Chem. Sci.*, 2019, **11**, 694-698.
12. M.-H. Lee, C.-H. Yang and J.-H. Jan, Band-resolved analysis of nonlinear optical properties of crystalline and molecular materials, *Phys. Rev. B*, 2004, **70**, 235110.
13. J. J. Zhang, Z. H. Zhang, W. G. Zhang, Q. X. Zheng, Y. X. Sun, C. Q. Zhang and X. T. Tao, Polymorphism of $BaTeMo_2O_9$: A new polar polymorph and the phase transformation, *Chem. Mater.*, 2011, **23**, 3752-3761.
14. H. Y. Chang, S. W. Kim and P. S. Halasyamani, Polar hexagonal tungsten oxide (HTO) materials: (1) Synthesis, characterization, functional properties, and structure−property relationships in $A_2(MoO_3)_3(SeO_3)$ ($A = Rb^+$ and Tl^+) and (2) Classification, structural distortions, and second-harmonic generating properties of known polar HTOs, *Chem. Mater.*, 2010, **22**, 3241–3250.